ISSN 1063-7826, Semiconductors, 2020, Vol. 54, No. 12, pp. 1577–1582. © Pleiades Publishing, Ltd., 2020.

SURFACES, INTERFACES, AND THIN FILMS

Influence of Annealing Temperature Variations on the Properties of Chemically Deposited Nanocrystalline Zinc Selenide Thin Films

T. A. H. Mir[a], R. A. G. Shaikh[a], D. S. Patil[a], and B. K. Sonawane[a,*]

[a] *Department of Electronics, School of Physical Sciences, Kavayitri Bahinabai Chaudhari North Maharashtra University, Jalgaon, Maharashtra, 425001 India*

**e-mail: sonawane@,rediffmail.com*

Received July 17, 2020; revised July 17, 2020; accepted August 13, 2020

Abstract—In the present report, influence of annealing temperature variations on the optical, morphological, and structural properties of chemically deposited nanocrystalline zinc-selenide thin films is studied employing an X-ray diffractometer, scanning electron microscope, and UV spectroscope. As-synthesized and annealed films exhibit nanocrystalline nature with cubic structure. The result shows that ZnSe thin films contain spherical particles that are composed of nanocrystals ranging from 3 to 7 nm crystallite size. The SEM studies reveal that the inter-crystalline spaces have been found to be reduced with an increase in grain size as annealing temperature increases. The EDS data reveal that the obtained thin films are rich in selenium. However, thermal annealing assisted to reduce the non-stoichiometric nature of the films by reducing selenium content that was found to be reduced with a rise in annealing temperature. The reduction in strains and dislocation density was observed after the annealing process. The band-gap energy was found to be raised from 2.56 to 2.76 eV with a rise in annealing temperature. The transmittance of more than 80% was recorded by as-synthesized and annealed films as well.

Keywords: chemical bath deposition, annealed ZnSe films, optical properties

DOI: 10.1134/S1063782620120234

1. INTRODUCTION

Zinc selenide II–VI group zinc chalcogenide has gained attention in the optoelectronic industry due to its brilliant properties like wide band gap, higher refractive index, and minimum optical absorption in the visible–infrared spectrum. The properties of this chalcogenide like band gap, film thickness, transmission and absorption wavelengths are explored to facilitate its use in solar cell applications [1]. One of the reasons for the inclusion of ZnSe in solar applications lies in the fact that cadmium being highly-toxic material [2, 3] that dominated the solar industry for a long time needs to be replaced by other suitable materials. The features of zinc selenide like wide band gap, good conduction band, better lattice matching with Cu(In, Ga)Se_2(CIGS)-based absorbers, and lesser toxicity make it a suitable candidate for solar-cell applications [4–6]. The various thin film fabrication methods such as pulsed laser deposition [7], physical vapor deposition [8], spray pyrolysis [9], successive ionic layer adsorption and reaction (SILAR) [10], sol–gel deposition [11], and chemical-bath deposition method [12–15] are available. The chemical-bath deposition method known for its simplicity, affordable laboratory investment, and low-temperature is suitable for large-area deposition, which makes it a popular method in solar cell-related applications. The several deposition parameters like concentration of precursors used, pH of reaction bath, nature of the complexing agent, annealing treatment, etc. influence properties of thin films [6]. Thermal annealing is one of the effective tools to enhance and tailor various optoelectronic properties of as-synthesized nanocrystalline thin films [16, 17]. ZnSe-based solar cells can achieve an efficiency of more than 11% [18, 19]. The photo-conversion efficiency is dependent on band gap [20, 21], which can be tuned to some extent by subjecting ZnSe films to annealing at different temperatures.

In the present investigation, a convenient chemical-bath deposition technique is employed to synthesize ZnSe thin films maintaining deposition temperature of 70°C. The films were subjected to annealing at various temperatures, and their structural, morphological, and optical characteristics were discussed and compared.

2. EXPERIMENTAL

ZnSe thin-film synthesis procedure begins with the preparation of a 100-ml stock solution that contains sodium seleno-sulfate as a Se_2- ion source. Refluxing 2.5 g of selenium with 7.5 g of sodium sulfate with continuous stirring for 8 h at a temperature of 80°C gives 100 mL of stock solution. A chemical solution con-

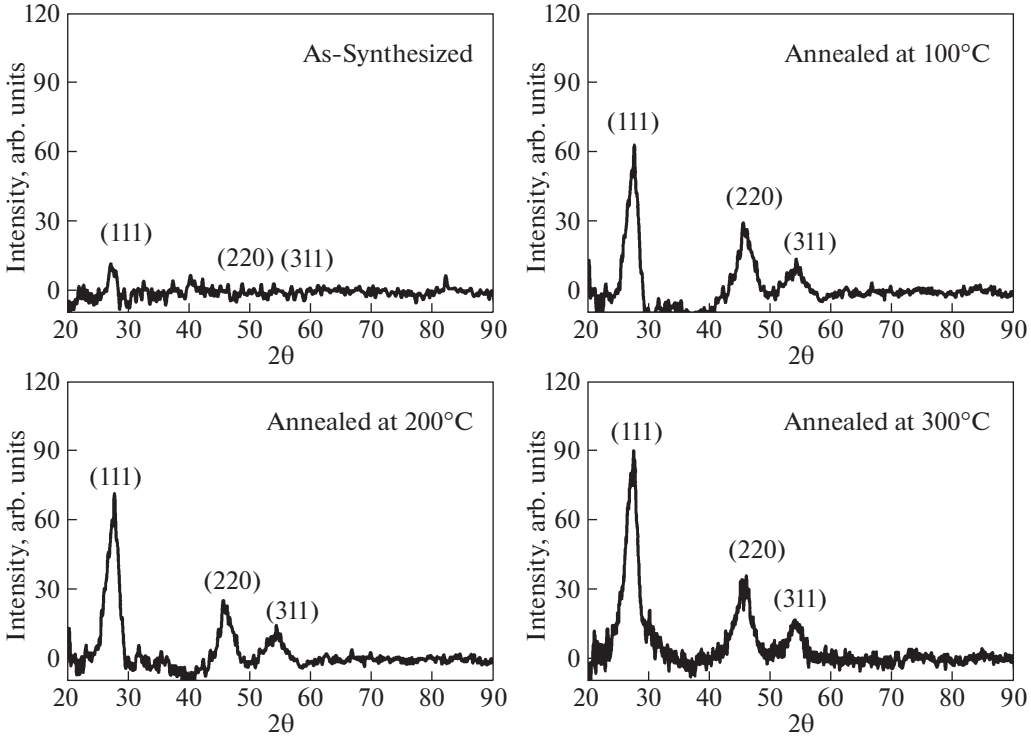

Fig. 1. XRD analysis of the as-synthesized and annealed ZnSe thin films at various annealing temperatures.

taining 10 mL (0.5 M) of zinc sulfate (Zn^{2+} ion source), 7 mL of 80% hydrazine hydrate, and 10 mL of 25% ammonia with 55 mL deionized water used for the deposition was subjected to a constant-temperature water bath controlled at 70°C. A 20 mL of filtered stock solution was added to it once the temperature of the bath reached 70°C. The pre-cleaned glass substrates were used for the deposition that lasted for 3 h. The post-deposition cleaned and dried substrates were annealed at different temperatures of 100, 200, and 300°C for an hour.

The crystallographic study of as-synthesized and annealed zinc-selenide thin films was done by X-ray diffractometer Philips PW3710 ($\lambda = 1.54056$ Å) in the 20 range of 20–90° with CuK_α radiation. The microscopic study and chemical composition of thin films were obtained from a scanning electron microscope (JEOL JED-2300 JAPAN) with the EDS (energy-dispersive X-ray spectroscopy) facility. The optical absorption spectra of the ZnSe thin films were obtained from spectrophotometer (UV-3600 SHIMADZU) for a spectral range of 300–800 nm.

3. RESULTS AND DISCUSSION

3.1. Structural Characterization

The XRD pattern of as-synthesized and annealed zinc selenide thin films was examined by an X-ray diffractometer in a range of 20–90° (Fig. 1).

From the literature survey, it is known that the two structural phases, namely, hexagonal wurtzite and cubic zinc blende are observed in zinc selenide [4]. In some cases, a mixture of both may be observed. In our report, as-synthesized ZnSe thin film does not exhibit well-resolved peaks in the XRD data, indicating amorphous nature. However, a weak intensity peak (111) is visible in the XRD pattern of the as-synthesized film. In all annealed films, characteristic peaks were observed at 27.82, 45.6, and 54.3o values of 2θ. These peaks are attributed to the (111), (220), and (311) planes, respectively, which shows the cubic phase with preferred orientation in (111) direction [JCPDS data file no. 80-0021]. The sharp peak (111) is due to the crystalline nature of the annealed films. With an increase in annealing temperature, the intensity of the dominant peak was found to be increased to some extent, which emphasizes that annealing is responsible for improving the crystallinity of the films. The narrowing of peaks was seen as annealing temperature increased, which was the indication of enhancement of crystallite size. The grain size is maximum (7 nm) for the ZnSe sample annealed at 300°C. The instrumental and physical factors (crystallite size and lattice strains) may cause the broadening of X-ray diffraction peak [22]. No other impurity peaks were observed for annealed samples. The results from XRD patterns were used to calculate the crystallite size D, the lattice parameter a, the lattice spacing d, the dislocation density δ, and the strain ε. XRD data analysis of

Table 1. XRD data analysis of as-synthesized and annealed ZnSe thin films at various annealing temperatures

Samples	2θ, deg	Planes (*hkl*)	FWHM β, rad	*D*, Å
As-synthesized	27.33	111	0.480	3.2624
100°C	27.82	111	0.376	3.2060
200°C	27.82	111	0.279	3.2060
300°C	27.82	111	0.211	3.2060

as-synthesized and annealed thin films for the (111) peak such as FWHM and *d* spacing are listed in Table 1.

The slight peak shift towards a higher 2θ value (27.82°) was observed for all annealed samples, which results in a decrease in inter-planar distance of (111) plane. The FWHM decreases with rise in annealing temperature, which reveals the grain size enhancement as annealing temperature increases. The lattice spacing *d* was estimated using Bragg's formula [23]

$$d = \frac{\lambda}{2\sin\theta},$$

where λ is the wavelength of X-ray used, θ is the Bragg's angle. The crystallite size *D* can be calculated using the Debye–Scherrer formula,

$$D = \frac{0.94\lambda}{\beta\cos\theta},$$

where β is full width at half maximum of the prominent peak. The enhancement of crystallite size was observed with rise in annealing temperature may be due to amalgamation of small crystals. The lattice parameter for the cubic structure is calculated by the following relation [24]:

$$\frac{1}{d^2} = \frac{h^2 + k^2 + l^2}{a^2}.$$

Here, *h*, *k*, *l* are lattice planes. The variations in lattice parameters imply the presence of strain in the grains of films that arise as a result of a change in nature and concentrations of native defects [25]. The dislocation density was calculated by using the following relation [26],

$$\delta = \frac{15\beta\cos\theta}{4aD}.$$

The strain (ε) in the films was calculated from the relation

$$\varepsilon = \frac{\beta\cos\theta}{4}.$$

The grain size, lattice parameter, strain, and dislocation density of as-synthesized and annealed films are summarized in Table 2.

The dislocation density and strain were found to be lowered with increase in annealing temperature suggesting an improvement in the crystallinity. From Tables 1 and 2, it is clear that the grain size is observed to be increased from 3 to 7 nm with increase in annealing. The surface defects like strain and dislocation density were reduced in annealed samples.

3.2. Elemental and Morphological Analysis

The EDS spectra of the as-synthesized and ZnSe thin film annealed at 300°C are depicted in Fig. 2 and their elemental study is listed in Table 3.

It is found that as-synthesized ZnSe thin film exhibits higher content of selenium. This is due to the presence of a considerably higher amount of hydrazine hydrate (7 mL) which acts as a strong reducing agent and is an essential element in ZnSe film growth [15, 27]. The absence of hydrazine hydrate results in a reduction in the conversion efficiency of solar cells [15, 28]. The present study shows that the atomic percentage of Zn:Se is 38.84:61.16 for as-synthesized films and 44.63:55.37 for the film annealed at 300°C. Thus there is a significant reduction in excessive Se content due to evaporation at the annealing temperature of 300°C. Thus with an increase in annealing temperature, a reduction in the non-stoichiometric nature of films was observed. Thermal annealing thus assisted in adjusting stoichiometry by removing excessive selenium by evaporation [29]. However, it is worth noting that all the films, as-synthesized and annealed, are selenium-rich.

As illustrated in Fig. 3, the SEM micrographs of all nanocrystalline samples exhibit a uniform distribution of spherical nanoclusters over the entire glass substrate.

It is seen that ZnSe spherical nanoclusters are distinguishable from each other with a smooth background. It is clear from EDS results that as the annealing temperature tends to increase, there is a reduction

Table 2. Grain size, lattice parameter, strain, and dislocation density of as-synthesized and annealed ZnSe thin films at various annealing temperature

Samples	Grain size, nm	Lattice parameter, Å	Strain, $\text{lin}^{-2}\,\text{m}^{-4}$	Dislocation density, $10^{16}/\text{m}^2$
As-synthesized	3.0	5.6505	0.114	9.96
100°C	3.9	5.5529	0.091	6.21
200°C	5.3	5.5529	0.067	3.42
300°C	7.0	5.5529	0.051	1.95

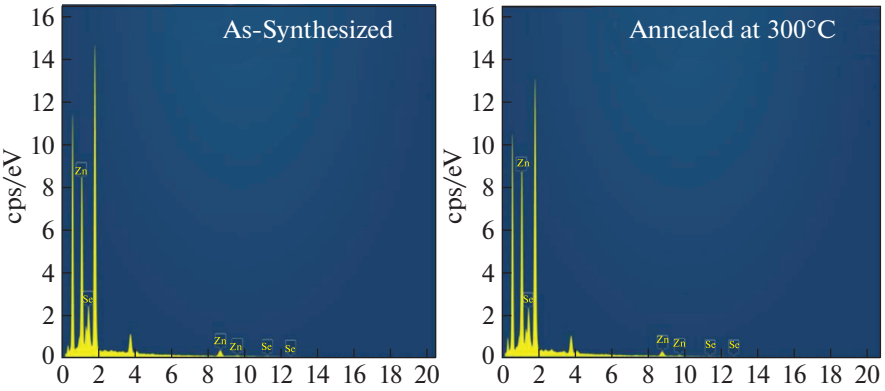

Fig. 2. EDS spectra of the as-synthesized and ZnSe film annealed at 300°C.

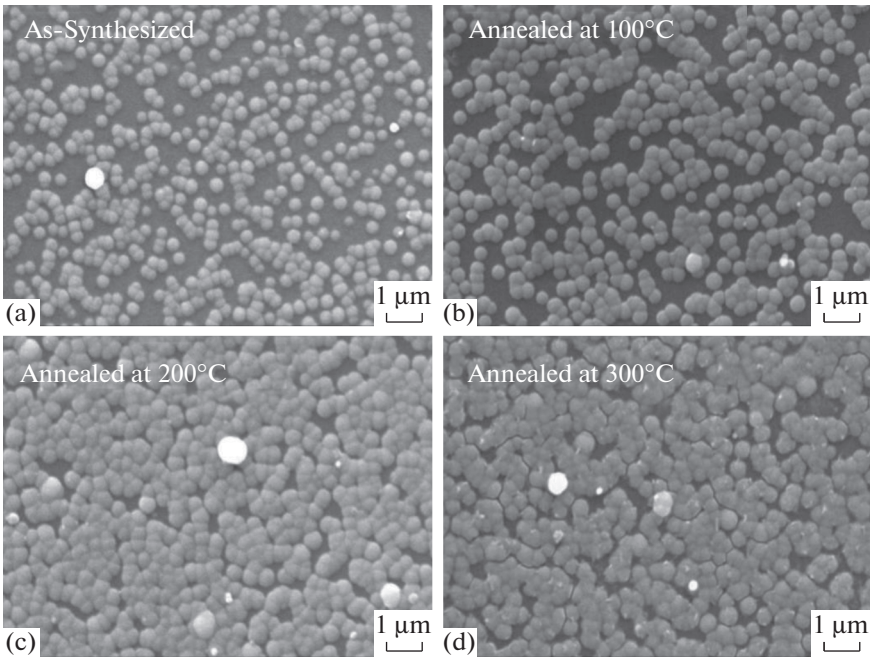

Fig. 3. SEM images of the as-synthesized and annealed ZnSe thin films at various annealing temperatures.

in excessive Se content due to evaporation, thus a decrease in lower-sized Se^{2-} (1.22 Å) and an increase in-higher sized Zn^{2+} (1.53 Å) results in an enhancement in crystallite size. It is seen from SEM micrographs that the sparing distribution of nanocrystals tends to diminish and the compact nature of nanocrystals is observed with an increase in annealing temperature. Thus the thermal annealing had an impact on the size and distribution of the film grains.

3.3. Optical Analysis

The optical absorption spectra of as-synthesized and annealed ZnSe thin films were obtained in the

Table 3. Elemental analysis

Elements	Line type	As-synthesized ZnSe		ZnSe annealed at 300°C	
		wt %	at %	wt %	at %
Zn	K series	34.45	38.84	40.02	44.63
Se	L series	65.55	61.16	59.98	55.37

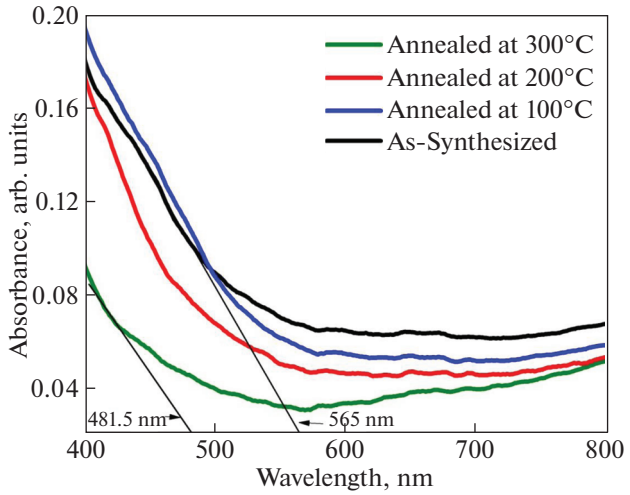

Fig. 4. Absorbance spectra of the as-synthesized and annealed ZnSe thin films at various annealing temperatures.

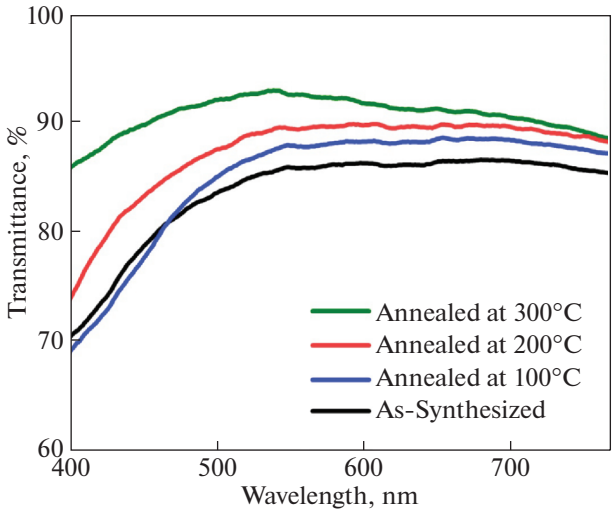

Fig. 5. Transmittance spectra of the as-synthesized and annealed ZnSe thin films at various annealing temperatures.

spectral range of 400–800 nm at room temperature as shown in Fig. 4.

The absorbance for both as-synthesized and annealed films is low and found to be decreased with rising annealing temperature. The obtained range of absorption edges from absorbance spectra is 481.5 nm (2.57 eV) to 565 nm (2.19 eV), which is in the visible range. The absorption edge shifts towards the lower wavelengths with the rise in annealing temperature. This blue shift causes an increase in crystallite size with rise in annealing temperature. The 460 nm is the standard value of the absorption edge of the bulk ZnSe. It is seen that with a rise in annealing temperature the absorption edge is approaching the bulk value of ZnSe.

The transmittance spectra of as-synthesized and annealed ZnSe thin films are plotted in Fig. 5.

It is clear from Fig. 5 that all the films, as-synthesized and annealed, show transmittance more than 80%. The transmittance was found to be increased with rise in annealing temperature. This high transmittance is one of the basic requirements of a buffer layer of solar cells [30]. The transition from the valence band to the conduction band is given by the fundamental absorption depicted by the following relation, and it helps to find out the band gap of the films. The band gap was obtained using following relation [31]:

$$\alpha = A\frac{(h\nu - E_g)^n}{h\nu},$$

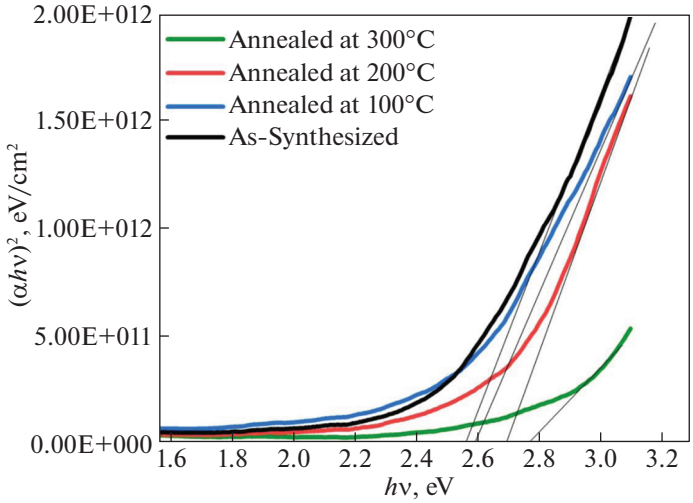

Fig. 6. Plot of $(\alpha h\nu)^2$ versus photon energy ($h\nu$) of the as-synthesized and annealed ZnSe thin films at various annealing temperatures.

where α is the absorption coefficient, A is a constant, n is equal to 1/2 for direct band gap semiconductor. The energy intercept of the plot $(\alpha h\nu)^2$ versus $h\nu$ as shown in Fig. 6 gives the band gap for the direct transition.

The band gap of the as-synthesized film was found to be 2.56 eV. There is a gradual increase in blue-shift in the band gap energy of ZnSe films (up to 2.76 eV) with the increase in annealing temperature. Similar blue shifts in band gap energy have been observed in earlier reports for thermally evaporated ZnSe thin films [17, 32]. It is worth noting that the film annealed at 200°C shows band gap energy (2.69 eV) closest to the bulk value of ZnSe.

4. CONCLUSIONS

Selenium-rich nanocrystalline zinc-selenide thin films have been synthesized by a chemical-bath deposition method. The EDS data confirms the reduction in the non-stoichiometric nature of films on annealing treatment. The XRD studies revealed narrowing of the peaks as annealing temperature was increased, with preferred orientation along (111), which is the indication of enhancement of crystallite size. SEM studies revealed the improvement in the crystallinity of annealed samples with an increase in grain size at the higher annealing temperature. It is found that band gap can be tuned with thermal annealing from 2.56 to 2.76 eV. The obtained range of band gap values and transmittance of more than 80% can be utilized to facilitate its use in solar-cell applications.

FUNDING

This research work is supported by the VCRMS (Vice-Chancellor Research Motivational Scheme), Kavayatri Bahinabai Chaudhari North Maharashtra University (NMU/11A/VCRMS/2016-17/Science1/85).

CONFLICT OF INTEREST

Authors have no conflict of interest to be declared.

REFERENCES

1. A. Ennaoui, S. Siebentritt, M. Ch. Lux-Steiner, W. Riedl, and F. Karg, Sol. Energy Mater. Sol. Cells **67**, 31 (2001).
2. J. Wennerberg, PhD Thesis (Uppsala Univ., Uppsala, Sweden, 2002).
3. I. Repins, M. A. Contreras, B. Egaas, C. DeHart, J. Scharf, C. L. Perkins, T. Bobby, and R. Noufi, Prog. Photovolt.: Res. Appl. **16**, 235 (2008).
4. C. D. Lokhande, P. S. Patil, H. Tributsch, and A. Ennaoui, Sol. Energy Mater. Sol. Cells **55**, 379 (1998).
5. M. Ganchev, N. Strahieva, E. Tzvetkova, and I. Gadjov, J. Mater. Sci. Mater. Electron. **14**, 847 (2003).
6. Y. Yan and M. M. Al-Jassim, Prog. Photovolt. **10**, 309 (2002).
7. G. Perna, V. Cappozi, M. C. Plantamura, A. Minafra, P. F. Biagi, S. Orlando, V. Marotta, and A. Giardini, Appl. Surf. Sci. **186**, 521 (2002).
8. G. I. Rusu, V. Ciupina, M. E. Popa, G. Prodan, G. G. Rusu, and C. Baban, J. Non-Cryst. Solids **352**, 1525 (2006).
9. M. Oztas and M. Bedir, Mater. Lett. **61**, 343 (2007).
10. R. B. Kale and C. D. Lokhande, Mater. Res. Bull. **39**, 1829 (2004).
11. H.-Q. Jiang, C. H. Jun, and Y. Xi, Trans. Non-Ferr. Met. Soc. **16**, 266 (2006).
12. L. P. Deshmukh, P. C. Pingale, S. S. Kamble, S. A. Lendave, S. T. Mane, B. R. Pirgonde, and M. Sharon, Mater. Lett. **92**, 308 (2013).
13. J. M. Dona and J. Herrero, J. Electrochem. Soc. **142**, 764 (1995).
14. H. Metin, S. Durmus, S. Erat, and M. Ari, Appl. Surf. Sci. **257**, 6474 (2011).
15. L. Chen, D. Zhang, G. Zhai, and J. Zhang, Mater. Chem. Phys. **120**, 456 (2010).
16. M. J. Kim, H. S. Lee, J. Y. Lee, T. W. Kim, K. H. Yoo, and M. D. Kim, J. Mater. Sci. **39**, 323 (2004).
17. M. Ashraf, S. M. J. Akhtar, A. F. Khan, Z. Ali, and A. Qayyum, J. Alloys Compd. **509**, 2414 (2011).
18. S. Siebentritt, T. Kampschulte, A. Bauknecht, U. Blieske, W. Harneit, U. Fiedeler, and M. Lux-Steiner, Sol. Energy Mater. Sol. Cells **70**, 447 (2002).
19. W. Eisele, A. Ennaoui, P. Schubert-Bischoff, M. Giersig, C. Pettenkofer, J. Krauser, M. Lux-Steiner, S. Zweigart, and F. Karg, Sol. Energy Mater. Sol. Cells **75**, 17 (2003).
20. M. F. Al-Kuhaili, A. Kayani, S. M. A. Durrani, I. A. Bakhtiari, and M. B. Haider, ACS Appl. Mater. Interface **5**, 5366 (2013).
21. M. Prabhu, Kamalakkannan, N. Soundararajan, and K. Ramachandran, J. Mater. Sci. Mater. Electron. **26**, 3963 (2015).
22. E. R. Shaaban, I. S. Yahia, N. Afify, G. F. Salem, and W. Dobrowolski, Mater. Sci. Semicond. Process. **19**, 107 (2014).
23. T. M. Khan, M. Zakria, M. Ahmad, and R. I. Shakoor, J. Lumin. **147**, 97 (2014).
24. C. Kittel, *Introduction to Solid State Physics* (Wiley, New York, 1996), Chap. 2.
25. S. Venkatachalam, D. Mangalaraj, S. K. Narayandass, K. Kim, and J. Yi, Phys. B (Amsterdam, Neth.) **358**, 27 (2005).
26. S. Venkatachalam, R. T. Rajendra Kumar, D. Mangalaraj, S. K. Narayandass, K. Kim, and J. Yi, Solid State Electron. **48**, 2219 (2004).
27. C. Mehta, G. S. S. Saini, J. M. Abbas, and S. K. Tripathi, Appl. Surf. Sci. **256**, 608 (2009).
28. A. M. Chaparro, M. T. Gutiérrez, J. Herrero, J. Klaer, M. J. Romero, and M. M. Al Jassim, Prog. Photovolt. Res. Appl. **10**, 465 (2002).
29. P. P. Hankare, P. A. Chate, D. J. Sathe, P. A. Chavan, and V. M. Bhuse, J. Mater. Sci. Mater. Electron. **20**, 374 (2009).
30. R. Sharma, S. L. Patel, S. Chander, M. D. Kannan, and M. S. Dhaka, Phys. Lett. A **384**, 126097 (2020).
31. K. M. Garadkar, A. A. Patil, P. P. Hankare, P. A. Chate, and D. J. Delekar, J. Alloys Compd. **487**, 786 (2009).
32. A. S. Hassanien, K. A. Aly, and A. A. Akl, J. Alloys Compd. **685**, 733 (2016).

SPELL: OK